An Improved Study of Electronic Band Structure and Optical Parameters of X-Phosphides (X=B, Al, Ga, In) by Modified Becke–Johnson Potential*

Masood Yousaf, M.A. Saeed, R. Ahmed, M.M. Alsardia, Ahmad Radzi Mat Isa, and A. Shaari

Physics Department, Faculty of Science, Universiti Teknologi Malaysia, UTM Skudai, 81310 Johor, Malaysia

(Received July 26, 2012; revised manuscript received August 30, 2012)

Abstract *We report the electronic band structure and optical parameters of X-Phosphides (X=B, Al, Ga, In) by first-principles technique based on a new approximation known as modified Becke–Johnson (mBJ). This potential is considered more accurate in elaborating excited states properties of insulators and semiconductors as compared to LDA and GGA. The present calculated band gaps values of BP, AlP, GaP, and InP are 1.867 eV, 2.268 eV, 2.090 eV, and 1.377 eV respectively, which are in close agreement to the experimental results. The band gap values trend in this study is as: E_g(mBJ-GGA/LDA) > E_g(GGA) > E_g(LDA). Optical parametric quantities (dielectric constant, refractive index, reflectivity and optical conductivity) which based on the band structure are also presented and discussed. BP, AlP, GaP, and InP have strong absorption in between the energy range 4–9 eV, 4–7 eV, 3–7 eV, and 2–7 eV respectively. Static dielectric constant, static refractive index and coefficient of reflectivity at zero frequency, within mBJ-GGA, are also calculated. BP, AlP, GaP, and InP show significant optical conductivity in the range 5.2–10 eV, 4.3–8 eV, 3.5–7.2 eV, and 3.2–8 eV respectively. The present study endorses that the said compounds can be used in opto-electronic applications, for different energy ranges.*

PACS numbers: 74.20.Pq, 74.25.Gz, 31.15.A-, 31.15.E-, 71.15.Mb
Key words: DFT, FP-LAPW + lo, mBJ-GGA, optical properties, electronic structure

1 Introduction

X-Phosphides (X=B, Al, Ga, In) binary compounds belonging to III-V semiconductors are under extensive study[1−4] in the recent years because of their useful physical, electro-optical and other distinctive properties.[1] They crystallize in zinc blend structure at ambient conditions; characterized by a single lattice constant.[1−2] BP, AlP, GaP are indirect band gap materials, and InP is a direct band gap semiconductor.

III-Phosphides have been utilizing in a number of opto-electronic devices operating at short wavelength range of the visible spectrum along with high temperature applications.[1] BP is categorized as a refractory material and possesses similar electronic structure like silicon carbide.[5−6] AlP is used particularly in IR (infrared) photo-detectors,[7] transferred-electron devices[7] and technologically significant for InP-AlP ternary system as the end points.[2] GaP is an applied material for LED (light emitting diodes).[1] InP is employed as a substrate for resonant interband tunneling diodes and high frequency field effect transistors.[8−9] InP nanowires and nanocrystals are potential materials for the solar cells.[10−12]

Precise measurements of the electronic band configuration and its dependent optical characteristics are required for the optimal device operation. Recently, the Perdew–Wang 91 (PW91) functional[13] was employed to these compounds and the band gap values were obtained using scissor operator.[1] It is worth mentioning that the band gaps values calculated in the present study are in a close agreement with the experimental results compared to other exchange correlation functional. The difference between present and other reported results is the first time use of a recent technique called "modified Becke Johnson Potential" (mBJ) to study these compounds. mBJ is known for overcoming the problem of band gaps' underestimation, in case of Local Density Approximation (LDA)[14] and Generalized Gradient Approximation (GGA).[13] Several studies have been conducted using mBJ potential to calculate the electronic properties of different families of solids. These studies corroborate that the said method gives much improved, and accurate band gaps energy values for a wide range of different materials.[15−19]

2 Method of Calculations

We have executed the computational work using FP-LAPW+lo (full potential linearized-augmented plane wave + local orbital) under the framework of DFT,[20] through the latest edition of WIEN2k software.[21] The mBJ (potential) is employed to minimize the shortcomings of GGA/LDA (approximations) in terms of misjudgment of the band gap value. The mBJ-GGA potential $V_{\rm xc}$[22] uses the mBJ exchange potential plus the GGA correlation potential and performs the calculation of band gaps

*Supported by (Foreign Academic Visitor Grant) of Universiti Teknologi Malaysia (UTM) Skudai, Johor, Malaysia for the Grant No. JI3000077264D035

© 2011 Chinese Physical Society and IOP Publishing Ltd

precisely, similar to the computationally expensive GW calculations. This method provides the band gaps' almost equal to the experimental values.

In the FP-LAPW + lo method, a unit cell is divided into an interstitial zone and non interweaving spheres known as muffin-tin (MT) of a specific radius (RMT). Inside the MT spheres, the basis sets are described by a linear combination of radial solutions of Schrodinger equation (for a single particle and at a fixed energy) along with the energy derivatives time spherical harmonics. Inside the each MT sphere, the set of basis is divided into subsets (core and valence). The spherically symmetric charge density core subsets are completely confined inside the MT sphere.

In the present study, a parameter determining the extent of secular matrix RMT*Kmax = 8 is used, where the RMT denotes the radius of muffin-tin (MT) sphere and Kmax is the associated value to the maximum K vector. The chosen parameter determines the matrix size. Fourier expansion of the charge density is carried up to Gmax = 14 $(\mathrm{Ry})^{1/2}$. The position of the first and second atom in zinc blend structure consisting of two FCC (Interpenetrating) sub-lattice is taken to be (0, 0, 0) and (0.25, 0.25, 0.25). The following states $3s^2 3p^3$, $4d^{10} 5s^2 5p^1$, $3d^{10} 4s^2 4p^1$, $3s^2 3p^1$, and $2s^2 2p^1$ for P, In, Ga, Al, and B respectively are considered as valence electrons. The MT radii of P, In, Ga, Al and B are adopted to be 1.8, 2.5, 2.2, 2.2 and 1.6 (a.u.) respectively. 700 K-points are used in first the Brillion zone for k-space integration to achieve self consistency. A number of iterations (40) are dedicated to accomplishing self consistency. Less than 0.000 01 Ry of total energy difference is used in per formula unit for succeeding iterations.

3 Results and Discussions

A comparative study of electronic band gaps with different exchange correlations energy functionals and optical traits involving the plots for dielectric's real and imaginary part, refractive index, extinction coefficient, reflectivity and optical conductivity of III-Phosphides binary compounds with mBJ-GGA is presented here.

Firstly, by minimizing the total energy with respect to the volume and fitting it to the Murnaghan equation of state,[23] equilibrium lattice constant a_0, the bulk modulus B_0 and the bulk modulus pressure derivative B' are evaluated. It is clear from Table 1 that our reported a_0 values are in a very close agreement with the experimental results. Here, we have just provided energy-volume curve (Fig. 1) of BP within FP-LAPW-LDA.

Band structures calculations are performed in the primitive brillouin zone along high symmetry directions as shown in Fig. 2. Calculated band structures of the compounds with mBJ-GGA, mBJ-LDA, GGA, and LDA are shown in Fig. 3. It is clear from the figures, that BP, AlP and GaP are indirect band gap materials while InP is a direct band gap compound. The present and previously calculated band gap results with GGA and LDA, deviate a little from each other, but underrate significantly from the experimental values. Whereas, the new mBJ-GGA/LDA potential has resolved this problem by providing the band gap values which are in good agreement with the experimental data (Table 2). The implementation of the mBJ-GGA/LDA has revealed the true intrinsic semiconductor character of these materials. Previously, the reason for not reporting the true nature of the band gap might be in the selection of exchange correlation functional. In all of the compounds, both mBJ-GGA and mBJ-LDA have produced almost the similar results. The unoccupied bands have shifted upward from Fermi level in case of mBJ-GGA/LDA resulting into the enhanced band gap as compared to GGA/LDA while retaining the similar shape and character of band structure.

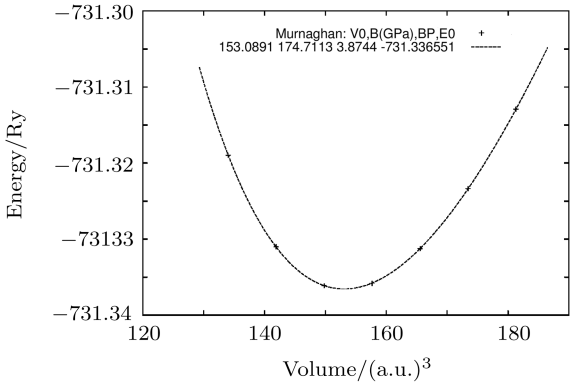

Fig. 1 Total energy-volume curve for BP within LDA.

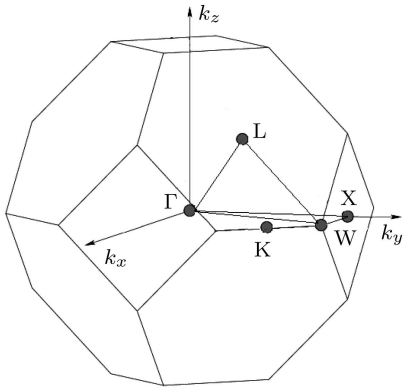

Fig. 2 Selected symmetric directions in primitive Brillouin zone.

To further explore the band gaps of materials, the total densities of states (TDOS) along with atomic site projected densities of states (PDOS) of BP, AlP, GaP and InP with mBJ-GGA are plotted in Fig. 4. We can specify the angular momentum character of different structures from PDOS. The Fermi level is set to be at 0 eV. In the case of mBJ-GGA, three different structures in DOS of these compounds appear separated from each other by gaps. Involvement of core state constitute lower valence band while upper valence band starts from −15 eV, −11.2 eV, −11.5 eV, and 11.1 eV in case of BP, AlP, GaP, and

InP respectively. The $2s^2 2p^1$(B), $3s^2 3p^1$(Al), $4s^2 4p^1$(Ga), and $5s^2 5p^1$(In) states are main contributors in the upper valence as well as in the lower conduction band of their respective compounds. Contribution from Ga-$3d^{10}$ of GaPand In–$4d^{10}$ of InP electrons is very small in the both valence and conduction band. BP, AlP, GaP and InP have strong localization region in upper valence band between −8.5 eV to −9.5 eV, −5 eV to −4 eV, −6.1 eV to −5.2 eV, and −5.1 eV to 4.3 eV respectively. In all of the studied compounds, localization of P–$3s^2$ is also visible in the lower valence band. Covalent interactions are apparent between the bonding elements due to degeneracy of states with regard to both lattice site and angular momentum.

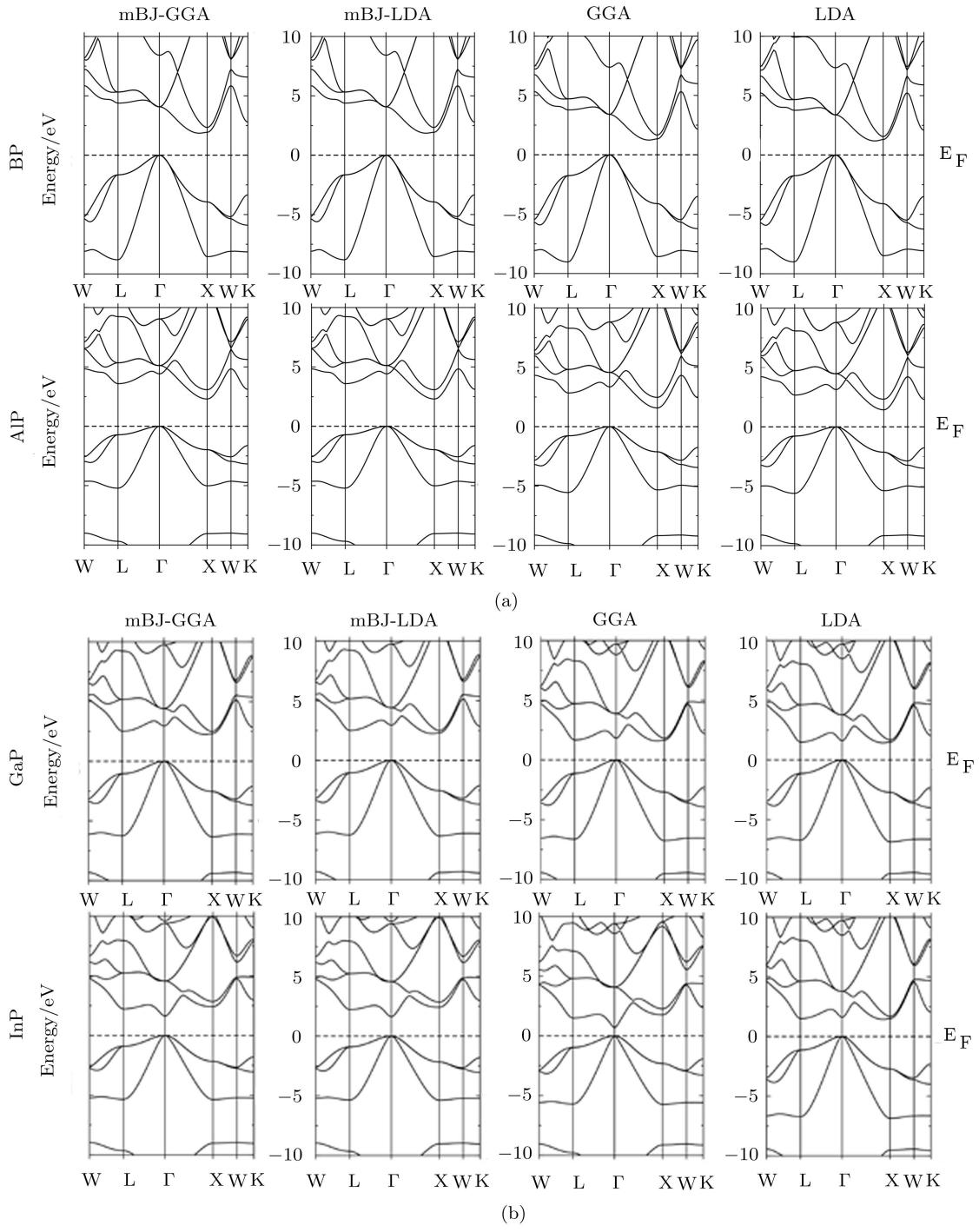

Fig. 3 (a) Band structures of BP and AlP within mBJ-GGA, mBJ-LDA, GGA, LDA. (b) Band structures of GaP and InP calculated within mBJ-GGA, mBJ-LDA, GGA, LDA.

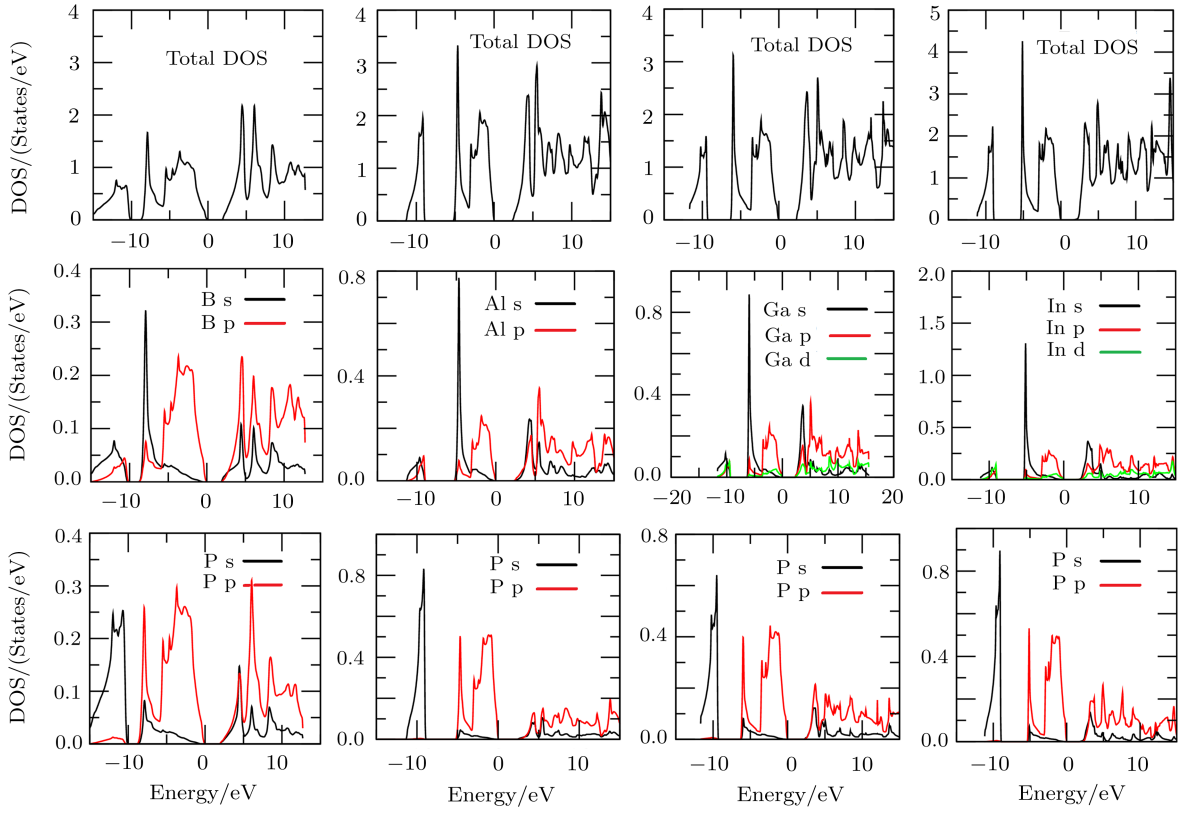

Fig. 4 Total and partial densities of states for BP, AlP, GaP and InP within mBJ-GGA.

Table 1 The lattice parameter (a), volume (V), bulk modulus (B) and its pressure derivative (B') of BP, AlP, GaP, and InP compounds.

Compounds	Method	a/Å	V/a.u.^{3}	B/GPa	B'
BP					
Present work	FP –GGA	4.481	159.0576	161.0079	3.7444
	FP –LDA	4.492	153.0981	174.7113	3.8744
Experiment	-	4.538[24]		173[25]	
Other calculations	FP-LDA	4.498[26]		176[26]	3.92[26]
	FP-GGA	4.555[26]		162[26]	3.86[26]
	PP-LDA	4.475[27]		172[27]	3.76[27]
	FP-GGA	4.546[28]		170[28]	
AlP					
Present work	FP-LAPW-GGA	5.506 737	283.0173	82.6285	3.9563
	FP-LAPW-LDA	5.440 139 2	271.9074	89.4455	4.1273
Experiment	-	5.451[24]		86[24]	
Other calculations	FP-LDA	5.436[26]		89[26]	4.14[26]
	FP-GGA	5.511[26]		82[26]	3.99[26]
GaP					
Present work	FPLAPW-GGA	5.512 970 0	282.9760	76.8234	4.2968
	FPLAPW-LDA	5.399 605	265.8741	89.5566	4.6089
Experiment	-	5.450[24]		91[24]	
Other calculations	FP-LDA	5.398[26]		91[26]	4.76[26]
	FP-GGA	5.512[26]		76[26]	4.60[26]
InP					
Present work	FPLAPW-GGA	5.972 385 6	359.7880	60.0923	4.4124
	FPLAPW-LDA	5.842 107 49	336.7510	70.9723	4.8076
Experiment	-	5.869[24]		72[24]	
Other calculations	FP-LDA	5.838[26]		71[26]	4.78[26]
	FP-GGA	5.968[26]		62[26]	4.04[26]

Table 2 The energy band gap (E_g) values of BSb, AlSb, GaSb, calculated within mBJ-GGA, mBJ-LDA, GGA, and LDA.

Compounds	Methods	XC	Eg/eV	Type of band-gap
BP				
Present work	FP-LAPW	mBJ-GGA	1.867	Indirect ($\Gamma - \Delta_{\min}$)
	FP-LAPW	mBJ-LDA	1.866	Indirect ($\Gamma - \Delta_{\min}$)
	FP-LAPW	GGA	1.275	Indirect ($\Gamma - \Delta_{\min}$)
	FP-LAPW	LDA	1.170	Indirect ($\Gamma - \Delta_{\min}$)
Experiment			2.10[24]	Indirect ($\Gamma - \Delta_{\min}$)
			2.00[29]	
Other calculations	PAW	PW91-GGA	1.38[1]	Indirect ($\Gamma - \Delta_{\min}$)
	FP-LAPW	GGA	1.24[26]	
	FP-LAPW	LDA	1.18[26]	Indirect ($\Gamma - \Delta_{\min}$)
AlP				
Present work	FP-LAPW	mBJ-GGA	2.268	Indirect (Γ-X)
	FP-LAPW	mBJ-LDA	2.267	Indirect (Γ-X)
	FP-LAPW	GGA	1.574	Indirect (Γ-X)
	FP-LAPW	LDA	1.438	Indirect (Γ-X)
Experiment			2.500[24]	Indirect (Γ-X)
Other calculations	PAW	PW91-GGA	1.73[1]	
	FP-LAPW	GGA	1.57	Indirect (Γ-X)
	FP-LAPW	LDA	1.44	Indirect (Γ-X)
GaP				
Present work	FP-LAPW	mBJ-GGA	2.090	Indirect ($\Gamma - \Delta_{\min}$)
	FP-LAPW	mBJ-LDA	2.090	Indirect ($\Gamma - \Delta_{\min}$)
	FP-LAPW	GGA	1.644	Indirect ($\Gamma - \Delta_{\min}$)
	FP-LAPW	LDA	1.491	Indirect ($\Gamma - \Delta_{\min}$)
Experiment			2.350[24]	Indirect ($\Gamma - \Delta_{\min}$)
Other calculations	PAW	PW91-GGA	1.62[1]	
	FP-LAPW	GGA	1.59[26]	Indirect ($\Gamma - \Delta_{\min}$)
	FP-LAPW	LDA	1.44[26]	Indirect ($\Gamma - \Delta_{\min}$)
InP				
Present work	FP-LAPW	mBJ-GGA	1.377	Direct ($\Gamma - \Gamma$)
	FP-LAPW	mBJ-LDA	1.374	Direct ($\Gamma - \Gamma$)
	FP-LAPW	GGA	0.684	Direct ($\Gamma - \Gamma$)
	FP-LAPW	LDA	0.453	Direct ($\Gamma - \Gamma$)
Experiment			1.424[24]	Direct ($\Gamma - \Gamma$)
Other calculations	PAW	PW91-GGA	1.86[1]	Direct ($\Gamma - \Gamma$)
	FP-LAPW	GGA	0.85[26]	Direct ($\Gamma - \Gamma$)
	FP-LAPW	LDA	0.62[26]	Direct ($\Gamma - \Gamma$)

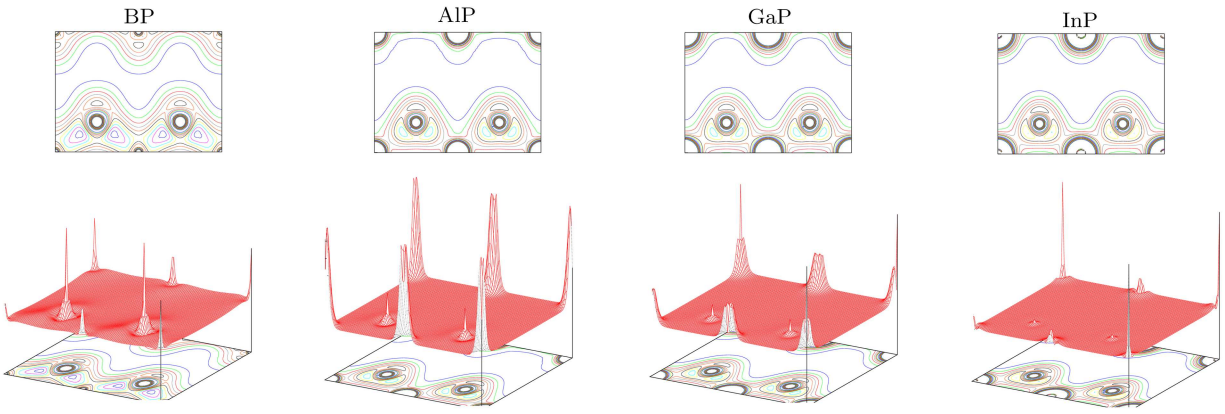

Fig. 5 The contour and 3D plots of BP, AlP, GaP and InP for electron density in the (110) plane.

To probe the bonding nature of constituent atoms, the contour and 3-D plots for electron density in the (110) plane are drawn (Fig. 5). Plots show a little ionic behavior as there is minute difference of electronegativity between the comprising elements. Therefore, the bonding may be expressed as a strong covalent behavior. BP shows the strongest while AlP shows the weakest covalent character of the studied compounds.

For cubic symmetry compounds $\varepsilon_2(\omega)$ (imaginary part of the complex dielectric function) can be calculated by the following relation:[30]

$$\varepsilon_2(\omega) = \frac{8}{2\pi\omega^2} \sum_{nn'} \int_{BZ} |P_{nn'}(k)|^2 \frac{\mathrm{d}S_k}{\nabla\omega_{nn'}(k)}, \qquad (1)$$

where $\omega_{nn'}$ is the joint density of states and $P_{nn'}$ is momentum matrix element which affect $\varepsilon_2(\omega)$ strongly. Kramers–Kronig relation gives the real part of the complex dielectric function $\varepsilon_1(\omega)$ from the imaginary part $\varepsilon_2(\omega)$:[31]

$$\varepsilon_1(\omega) = 1 + \frac{2}{\pi} P \int_0^{\infty} \frac{\omega' \varepsilon_2(\omega')}{\omega'^2 - \omega^2} \mathrm{d}\omega' . \qquad (2)$$

The dielectric function's imaginary part is calculated in the energy range 0–30 eV within mBJ-GGA as shown in Fig. 6. Transitions from the top of the valence bands to the conduction bands at the lower states, contribute to the optical spectra's major part.[32] The first critical point (optical absorption's edge) in BP, AlP, GaP, and InP occurs at about 1.867 eV, 2.268 eV, 2.090 eV, and 1.377 eV for mBJ-GGA. BP, AlP, GaP and InP have strong absorption in between energy range 4–9 eV, 4–7 eV, 3–7 eV, 2–7 eV respectively. This region is represented by different peaks due to electronic transitions between the valence and conduction band. The absorption region has variation in the energy range (as mentioned previously) that depicts the appropriateness for device applications as these compounds can be operated within diverse segments of the spectrum.

Figure 7 shows the computed real portion of the dielectric function $\varepsilon_1(\omega)$. Static dielectric constants $\varepsilon_1(0)$ and $\varepsilon_1(\omega)$ in low energy limit strongly depends on the semiconductors' band gap. Penn model relating the inverse relation of $\varepsilon_1(0)$ with the band gap[33] is used i.e.

$$\varepsilon(0) \approx 1 + (\hbar\omega_p/\mathrm{E}_g)^2 . \qquad (3)$$

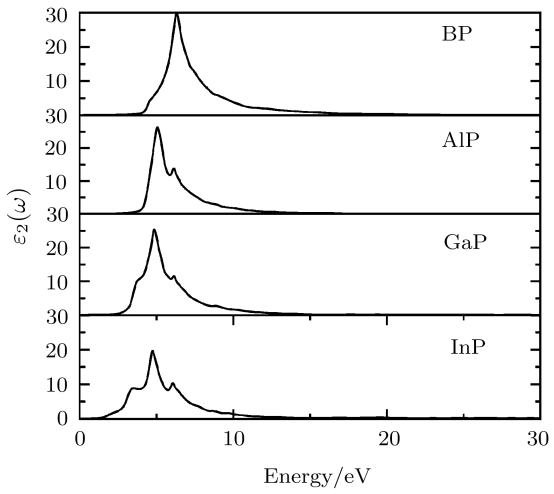

Fig. 6 Imaginary part of the dielectric function (Frequency dependent) of BP, AlP, GaP and InP within mBJ-GGA.

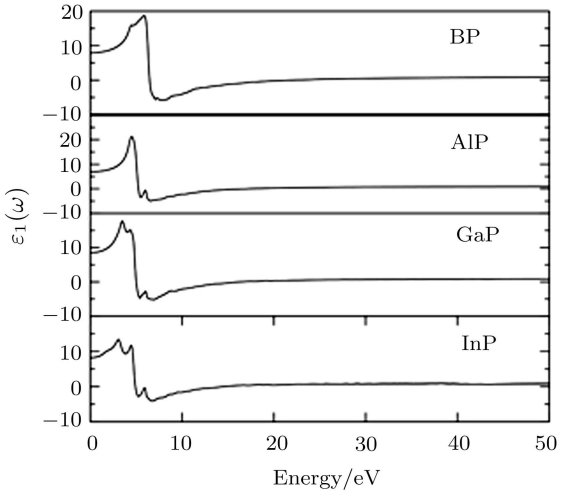

Fig. 7 Frequency dependent real part of dielectric functions of BSb, AlSb, GaSb and InSb within mBJ-GGA.

Table 3 Calculated static dielectric constant $\varepsilon_1(0)$, static refractive index $n(0)$ and coefficient of reflectivity at zero frequency $R(0)$ for BP, AlP, GaP, and InP within mBJ-GGA.

Compound	Methods	XC	$\varepsilon_1(0)$	$n(0)$	$R(0)$
BP	FP-LAPW	mBJ-GGA	7.902 56	2.8116	2.258 44
AlP	FP-LAPW	mBJ-GGA	6.924 27	2.631 42	2.018 33
GaP	FP-LAPW	mBJ-GGA	8.523 76	2.919 58	2.398 54
InP	FP-LAPW	mBJ-GGA	8.196 68	2.863 02	2.325 95

Using the value of $\varepsilon_1(0)$ and plasma energy $\hbar\omega$ in the above relation, the band gap value E_g can be calculated. The static dielectric constant values of BP, AlP, GaP and InP measured with the mBJ-GGA exchange correlations are listed in Table 3. With the mBJ-GGA, it is clear from Fig. 6 that $\varepsilon_1(\omega)$ initially increases up to the energy values maximum 5.8 eV, 4.4 eV, 3.4 eV, and 3.1 eV for BP, AlP, GaP, and InP respectively and afterward decreases to the smallest (negative) value at 7.8 eV, 6.7 eV, 6.9 eV, and 6.8 eV for BP, AlP, GaP and InP respectively. The values

lower than "1" for $\varepsilon_1(\omega)'$, exhibit the reflectiveness of material for the incident waves (electromagnetic) displaying a metallic character inside this energy range for these materials. So these materials can be used as a protection from radiations in this specific energy limits. The local maxima of reflectivity as shown in Fig. 9 attribute to the negative values of $\varepsilon_1(\omega)$. Additional increase in the energy to high value brings steadiness to $\varepsilon_1(\omega)$. The stable behavior after 10 eV suggests that the studied materials do not interact with these high energy photons as being transparent to them and thus are suitable for manufacturing lenses.

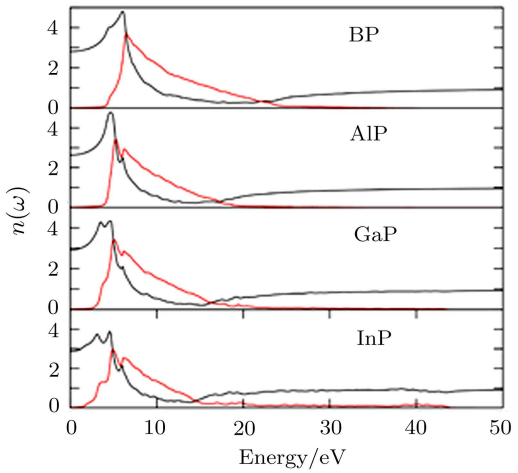

Fig. 8 Frequency dependent refractive index (upper line) and extinction coefficient (lower line) of BP, AlP, GaP and InP within mBJ-GGA.

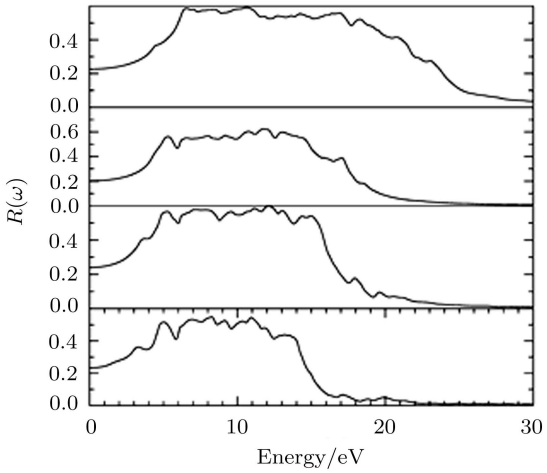

Fig. 9 Reflectivity (frequency dependent) of BP, AlP, GaP and InP within mBJ-GGA.

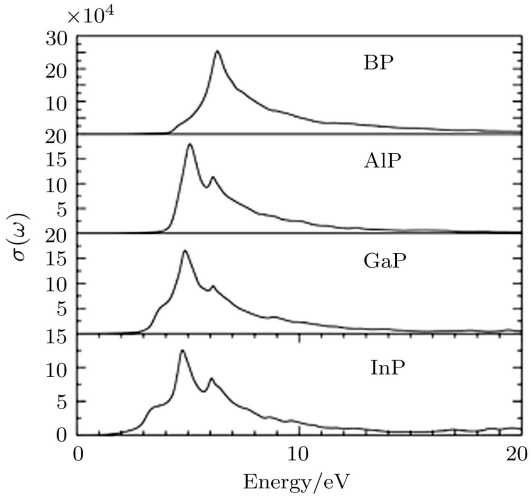

Fig. 10 Optical conductivity (frequency dependent) of BSb, AlSb, GaSb and InSb within mBJ-GGA.

Figure 8 (upper line) shows a broad spectrum of refractive index $n(\omega)$, for longer range of energy (0–50 eV). The index $n(\omega)$ closely follows to the real part of the complex dielectric function $\varepsilon_1(\omega)$.[34] Refractive index spectra of III-Phosphides show two significant features; figure shows that $n(\omega)$ reaches the highest value at around 4.8 at 6.1 eV, 4.79 at 4.6 eV, 4.32 at 4.7 eV and 4.89 at 4.5 eV for BP, AlP, GaP, and InP respectively with mBJ-GGA. Afterwards, the spectrum of $n(\omega)$ falls down at intermediate energies and then disappears at higher energies, because considered materials absorb high energy photons and cannot behave as transparent material. Figure 8 (upper line) depicts that the refractive index is less than "1" for the number of frequencies, showing a lower value of light celerity c than the light phase velocity that seems a disagreement to the relativity. The signal propagates in a dispersive medium with the group velocity v_g, ($v_g = \mathrm{d}\omega/\mathrm{d}k$) rather than at phase velocity ($v = \omega/k = c/n$). The equation relating v_g and v is given by:

$$v_g = v\left(1 - \frac{k}{n}\frac{\mathrm{d}n}{\mathrm{d}k}\right). \tag{4}$$

The above equation describes that v_g is always smaller than v. When a signal is transmitted in a spectral region, where v is greater than c, v_g is found to be less than c.[34] The static refractive index $n(0)$ values with mBJ-GGA are presented in Table 3.

Figure 8 (lower line) shows a relation between the extinction coefficient $k(\omega)$ and energy. The response of $k(\omega)$ and $\varepsilon_2(\omega)$ is very close to each other and according to the existing studies.[34] A small variation of $k(\omega)$ from $\varepsilon_2(\omega)$ is possible in a medium with little absorption coefficient.[34]

Figure 9 shows relationship between reflectivity (frequency dependent) $R(\omega)$ and energy with the mBJ-GGA. The magnitude of the reflectivity coefficients for BP, AlP, GaP, and InP at zero frequency are given in Table 3. The maximum value of reflectivity (peaks) which arises from the inter band transition are in the energy range 6–20 eV (BP), 4–15 eV (AlP), 4–16 eV (GaP), and 4.5–14 eV (InP). Possession of reflectivity in a specific frequency (energy); reflectivity variance along energy is appropriate for reflector.

The optical conductivity (frequency dependent) $\delta(\omega)$ for III-Phosphides is shown in Fig. 10. BP, AlP, GaP, and InP show a significant optical conductivity in the range

5.2–10 eV, 4.3–8 eV, 3.5–7.2 eV, and 3.2–8 eV respectively. All of the materials show sharp rise in conductivity with small energy change, reaching the highest value at 6.3 eV, 5.1 eV, 4.8 eV, 4.7 eV for BP, AlP, GaP, and InP respectively. BP has the maximum optical conductivity among these materials. Afterwards it decreases swiftly with the energy and becomes stable for higher energy range indicating that the material does not interact with photons.

4 Conclusions

Much improved Optoelectronic properties of X-Phosphides (B, Al, Ga, In) have been calculated by using a new technique known as modified Becke Johnson potential. We report first time, a much accurate study of electronic band structure and their dependent optical parameters of these compounds. Calculated band gaps of BP. AlP, GaP, and InP are 1.867 eV, 2.268 eV, 2.090 eV, and 1.377 eV respectively which are in very close agreement to the experimental results. Our study has the following trend for the band gap results: E_g(mBJ-GGA/LDA) > E_g(GGA)> E_g(LDA). Optical parametric quantities (dielectric constant, refractive index, reflectivity and optical conductivity), which strongly depend on the band structure results are also presented and examined. BP, AlP, GaP, and InP have strong absorption in between the energy range 4–9 eV, 4–7 eV, 3–7 eV, 2–7 eV respectively. Calculated static dielectric constant ε_1 (0), static refractive index $n(0)$ and coefficient of reflectivity at zero frequency $R(0)$ for these materials within mBJ-GGA are also presented. BP, AlP, GaP, and InP show a significant optical conductivity in the energy range 5.2–10 eV, 4.3–8 eV, 3.5–7.2 eV, and 3.2–8 eV respectively. This comprehensive and improved study endorses the applications of these materials in the optoelectronic devices.

References

[1] Z.Y. Jiao, S.H. Ma, and Y.L. Guo, Comp. Theor. Chem. **970** (2011) 79.

[2] A. Bouhemadou, R. Khenata, M. Kharoubi, T. Seddik, A.H. Reshak, and Y. AlDouri, Comp. Mater. Sci. **45** (2009) 474.

[3] W. Zhang, W. Wub, and X. Cheng, Physica B **405** (2010) 4536.

[4] O. Arbouche, B. Belgoumène, B. Soudini, Y. Azzaz, H. Bendaoud, and K. Amara, Comp. Mater. Sci. **47** (2010) 685.

[5] E. Schroten, A. Geossens, and J. Schoonman, J. Appl. Phys. **83** (1998) 1660; and references therein.

[6] R.M. Wentzcovitch and M.L. Cohen, J. Phys. C: Solid State Phys. **19** (1986) 6791.

[7] A.A. Ketterson, W.T. Masselink, J.S. Gedymin, J. Klem, C.K. Peng, W.F. Kopp, H. Morkoc, and K.R. Gleason, IEEE Trans. Electron. Dev. ED-33 (1986) 564.

[8] J.D. Werking, C.R. Chang, L.D. Chang, C. Nguyen, and H. Kroemer, IEEE Electron. Dev. Lett. **13** (1992) 164.

[9] J.R. Soderstrom, D.H. Chow, and T.C. McGill, Appl. Phys. Lett. **55** (1989) 1094.

[10] J.G. Díaz, G.W. Bryant, W. Jaskólski, and M. Zieliński, Phys. Rev. B **75** (2007) 245433.

[11] J. Carrete, R.C. Longo, L.M. Varela, J.P. Rino, and L.J. Gallego, Phys. Rev. B **80** (2009) 155408.

[12] T.J. Coutts and S. Naseem, Appl. Phys. Lett. **46** (1985) 164.

[13] J.P. Perdew, K. Burke and M. Emzerhof, Phys. Rev. Lett. **77** (1996) 3865.

[14] J.P. Perdew and Y. Wang, Phys. Rev. B **45** (1992) 13244.

[15] M. Yousaf, M.A. Saeed, A.R.M. Isa, A. Shaari, and H.A.R. Aliabad, Chin. Phys. Lett. **29** (2012) 107401.

[16] S.D. Guo and B.G. Liu, Europhys. Lett. **93** (2011) 47006.

[17] W. AlSawai, H. Lin, R.S. Markiewicz, L.A. Wray, Y. Xia, S.Y. Xu, M.Z. Hasan, and A. Bansil, Phys. Rev. B **82** (2010) 125208.

[18] W. Feng, D. Xiao, Y. Zhang, and Y. Yao, Phys. Rev. B **82** (2010) 235121.

[19] D.J. Singh, Phys. Rev. B **82** (2010) 205102.

[20] W. Kohn and L.S. Sham, Phys. Rev. B **140** (1965) A1133.

[21] P. Blaha, K. Schwarz, G. Madsen, D. Kvasnicka, and J. Luitz, Institute of Material Chemistry, TU Vienna. http://www.wien2k.at/.

[22] F. Tran and P. Blaha, Phys. Rev. Lett. **102** (2009) 226401.

[23] F.D. Murnaghan, Proc. Nat. Acad. Sci. USA **30** (1944) 244.

[24] R.W.G. Wyckoff, *Crystal Structures*, 2nd ed., Krieger, Malabar (1986).

[25] O. Madelung, *Semiconductors: Data Handbook*, Springer, Berlin (2004).

[26] R. Ahmed, Fazal-e-Aleem, S.J. Hashemifar, and H. Akbarzadeh, Physica B **403** (2008) 1876.

[27] S. Kalvoda, B. Paulus, P. Fulde, and H. Stoll, Phys. Rev. B **55** (1997) 4027.

[28] H. Meradji, S. Drablia, S. Ghemid, H. Belkhir, B. Bouhafs, and A. Tadjer, Phys. Stat. Sol. B **241** (2004) 2881.

[29] B. Paulus, P. Fulde, and H. Stoll, Phys. Rev. B **54** (1996) 2556.

[30] B. Amin, I. Ahmad, M. Maqbool, S. GoumriSaid, and R. Ahmad, J. Appl. Phys. **109** (2011) 023109.

[31] F. Wooten, *Optical Properties of Solids*, Academic Press, New York (1972).

[32] N.J. Van der Laag, M.D. Snel, P.C.M. Magusin, and G. de With, J. Eur. Ceram. Soc. **24** (2004) 2417.

[33] D. Penn, Phys. Rev. B **128** (1962) 2093.

[34] M. Fox, *Optical Properties of Solids*, Oxford University Press, Oxford (2001).